

# The Hidden Label-marginal Biases of Segmentation Losses

Bingyuan Liu<sup>1\*</sup>, Jose Dolz<sup>1</sup>, Adrian Galdran<sup>2</sup>, Riadh Kobbi<sup>3</sup>,  
Ismail Ben Ayed<sup>1</sup>

<sup>1</sup> ÉTS Montreal, Canada

<sup>2</sup> Universitat Pompeu Fabra, Barcelona, Spain

<sup>3</sup> Diagnos Inc., Canada

**Abstract.** Most segmentation losses are arguably variants of the Cross-Entropy (CE) or Dice losses. On the surface, these two categories of losses (i.e., distribution based vs. geometry based) seem unrelated, and there is no clear consensus as to which category is a better choice, with varying performances for each across different benchmarks and applications. Furthermore, it is widely argued within the medical-imaging community that Dice and CE are complementary, which has motivated the use of compound CE-Dice losses. In this work, we provide a theoretical analysis, which shows that CE and Dice share a much deeper connection than previously thought. First, we show that, from a constrained-optimization perspective, they both decompose into label-marginal penalties and closely related ground-truth matching penalties. Then, we provide bound relationships and an information-theoretic analysis, which uncover hidden label-marginal biases: Dice has an intrinsic bias towards specific extremely imbalanced solutions, whereas CE implicitly encourages the ground-truth region proportions. Our theoretical results explain the wide experimental evidence in the medical-imaging literature, whereby Dice losses bring improvements for imbalanced segmentation. It also explains why CE dominates natural-image problems with diverse class proportions, in which case Dice might have difficulty adapting to different label-marginal distributions. Based on our theoretical analysis, we propose a principled and simple solution, which enables to control explicitly the label-marginal bias. Our losses integrate CE with explicit terms based on  $\mathcal{L}_1$  or the KL divergence, which encourage label marginals to match target class proportions, thereby mitigating class imbalance but without losing generality. Comprehensive experiments and ablation studies over different losses and applications validate our theoretical analysis, as well as the effectiveness of our explicit label-marginal terms.

**Keywords:** segmentation, medical image segmentation, loss function

## 1 Introduction

Semantic segmentation is one of the most investigated problems in computer vision, and has been impacting a breadth of applications, from natural-scene

---

\* Corresponding author: bingyuan.liu@etsmtl.ca

understanding [5,14] to medical image analysis [17,6]. The problem is often stated as a pixel-wise classification, following the optimization of a loss function expressed with summations over the ground-truth regions, as in the standard Cross-Entropy (CE) loss. A challenging aspect of segmentation problems is the existence of extremely diverse distributions (or proportions of the segmentation regions) across different classes and instances. A representative example is the popular Cityscapes dataset [5], where the average proportions of some classes, such as *motorcycle* or *bicycle*, are below 1%, while the proportions of some classes, like *road* and *building*, can be larger than 10%. Therefore, the segmentation methods should be able to address the extreme class imbalance issue (small-region terms are nearly neglected in the objective), without losing generality to adapt to medium-to-large regions. In these scenarios, besides specifically designed deep-network architectures or training schemes [24,2], the loss function to be minimized during learning plays a critical role, and has triggered a large body of research works in the recent years [18,12,16,11,26,19,21].

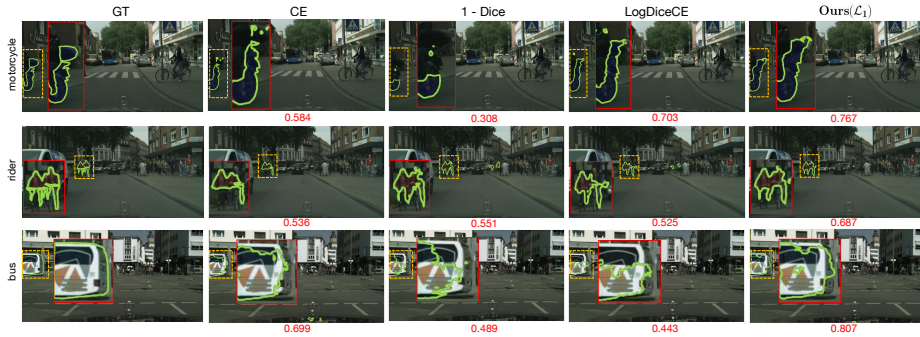


**Fig. 1. Visual illustrations of the improvements our solution brings over various CE-Dice losses under different class-imbalance scenarios in Cityscapes.** The ground-truth is given in the left-most column, and a magnified contour of the segmentation is provided alongside the target. The value below each image indicates the IoU score for the corresponding prediction. The examples show how Dice has a bias towards small regions, while CE is more stable for different scenarios. Our solution is capable of leveraging the best aspects of both. See Sec. 2 for an explicit theoretical analysis and Sec. 3 for detailed experiments. Best seen in color.

While there exists a great diversity of loss functions for segmentation, the recent excellent survey in [18] pointed to strong connections between these losses; see Fig. 1 in [18]. Most of the existing segmentation losses are arguably variants of the CE, Dice loss [18,28] or combinations of both [26,22], and could be categorized into two main families. The first family is motivated by distribution measures, i.e., CE and its variants, and is directly adapted from classification tasks. To deal with class imbalance, various extensions of CE have been investigated, such as increasing the relative weights for minority classes [20], or modifying the loss so as to account for performance indicators during training, as in the popular Focal loss [16] or TopK loss [27]. The second main family of losses is inspired by geometrical metrics. In this category, the most popular losses

are linear Dice [19] and its extensions, such as the logarithmic [26] or generalized [21] Dice loss. Borrowing the idea of the weighted CE, the latter introduces class weights to increase the contributions of the minority classes. These loss functions are motivated by the geometric Dice coefficient, which measures the overlap between the ground-truth and predicted segmentation regions.

In the literature, to our knowledge, there is no clear consensus as to which category of losses is better, with the performances of each varying across data sets and applications. It has been empirically argued that the Dice loss and its variants are more appropriate for extreme class imbalance, and such empirical observations are the main motivation behind the wide use and popularity of Dice in medical-imaging applications [19,9]. CE, however, dominates most recent models in the context of natural images [4,30,31,29]. Therefore, beyond experimental evidence, there is a need for a theoretical analysis that clarifies which segmentation loss to adopt for a given task, a decision that affects performance significantly.

On the surface, these two categories of losses (i.e., distribution based vs. geometry based) seem unrelated. Furthermore, it is widely argued within the medical imaging community that Dice and CE are complementary losses, which has motivated the use of compound CE-Dice losses integrating both [18,8,26,22]. These recent works, among many others, provided an intensive experimental evidence that points to highly competitive performances of compound CE-Dice losses, in a variety of class-imbalance scenarios. In particular, the recent comprehensive experimental study in [18] corroborated this finding with evaluations over more than 20 recent segmentation losses.

In this paper, we provide a constrained-optimization perspective showing that, in fact, CE and Dice share a much deeper connection than previously thought: They both decompose into label-marginal penalties and closely related ground-truth matching penalties. Our theoretical analysis highlights encoded hidden label-marginal biases in Dice and CE, and shows that the main difference between the two types of losses lies essentially in those label-marginal biases: Dice has an intrinsic bias preferring very small regions, while CE implicitly encourages the right (ground-truth) region proportions. Our results explain the wide experimental evidence in the medical-imaging literature, whereby using or adding Dice losses brings improvements for imbalanced segmentation with extremely small regions. It also explains why CE dominates natural-image problems with diverse class proportions, in which case Dice might have difficulty adapting to different label-marginal distributions (see Table 4 and the examples depicted in Fig. 1). Based on our theoretical analysis, we propose principled and simple loss functions, which enable to control explicitly the label-marginal bias. Our solution integrates the benefits of both categories of losses, mitigating class imbalance but without losing generality, as shown in the examples in Fig. 1.

Our contributions are summarized as follows:

- Showing through an explicit bound relationship (Proposition 1) that the Dice loss has a hidden label-marginal bias towards specific extremely imbal-

anced solutions, preferring small structures, while losing the flexibility to deal effectively with arbitrary class proportions.

- Providing an information-theoretic perspective of CE, via Monte-Carlo approximation of the entropy of the learned features (Proposition 2). This highlights a hidden label-marginal bias of CE, which encourages the proportions of the predicted segmentation regions to match the ground-truth proportions.

- Introducing new loss functions to control label-marginal biases: Our losses integrate CE with explicit terms based on  $\mathcal{L}_1$  or the KL divergence, which encourage label marginals to match target class proportions.

- Comprehensive experiments and ablation studies over different losses and applications, including natural and medical-imaging data, validate our theoretical analysis, as well as the effectiveness of our explicit label-marginal regularizers.

## 2 Formulation

**Table 1. Notations, formulations and approximations used in this paper.**  $\mathcal{F}$  and  $\mathcal{K}$  denotes the random variables associated with the learned features and the labels, respectively.  $\mathbb{P}$  denotes probability.  $|\cdot|$  denotes cardinality when the input is a set and the standard absolute value when the input is a scalar. Note that network parameters  $\theta$  are omitted in the prediction quantities, so as to simplify notations, as this does not lead to ambiguity.

Dataset		Modeling	
Concept	Formula	Concept	Formula
Indices/number of classes	$1 \leq k \leq K$	Model parameters	$\theta$
Spatial image domain	$\Omega \subset \mathbb{R}^2$	Feature embedding at pixel $i \in \Omega$	$\mathbf{f}_i^\theta$
Labels of pixel $i \in \Omega$	$y_{ik} \in \{0, 1\}$	Softmax predictions at pixel $i \in \Omega$	$p_{ik} = \mathbb{P}(k \mathbf{f}_i^\theta)$
GT region $k$	$\Omega_k = \{i \in \Omega   y_{ik} = 1\}$	Predicted proportion of class $k$	$\hat{p}_k = \frac{1}{ \Omega } \sum_{i \in \Omega} p_{ik}$
GT proportion of region $k$	$\hat{y}_k = \frac{ \Omega_k }{ \Omega }$	Predicted label-marginal prob.	$\mathbf{p} = (\hat{p}_k)_{1 \leq k \leq K}$
GT label-marginal prob.	$\mathbf{y} = (\hat{y}_k)_{1 \leq k \leq K}$	$(K-1)$ -simplex	$\Delta_K = \{\mathbf{p} \in [0, 1]^K / \sum_k \hat{p}_k = 1\}$

Losses, label-marginal regularizers and information-theoretic quantities	
Concept	Formula
Weighted cross-entropy	$\text{CE} = - \sum_{k=1}^K \frac{1}{ \Omega_k } \sum_{i \in \Omega_k} \log(p_{ik})$
Dice coefficient for region $k$	$\text{Dice}_k = \frac{2 \sum_{i \in \Omega_k} p_{ik}}{\sum_{i \in \Omega} p_{ik} +  \Omega_k }$
Label-marginal KL divergence	$\mathcal{D}_{\text{KL}}(\mathbf{y}    \mathbf{p}) = \sum_{k=1}^K \hat{y}_k \log(\frac{\hat{y}_k}{\hat{p}_k})$
Label marginal $\mathcal{L}_1$ distance	$\mathcal{L}_1(\mathbf{y}, \mathbf{p}) = \sum_{k=1}^K  \hat{y}_k - \hat{p}_k $
Monte-Carlo estimate of the entropy of features given region $k$	$\mathcal{H}(\mathcal{F}   \mathcal{K} = k) \approx - \frac{1}{ \Omega_k } \sum_{i \in \Omega_k} \log(\mathbb{P}(\mathbf{f}_i^\theta   k))$

Semantic segmentation is often stated as a pixel-wise classification task, following the optimization of a loss function for training a deep network. In Table 1, we present the notations, formulations and approximations used in our subsequent discussions. Besides the basic notations of the task (such as networks predictions), we explicitly include the loss functions, label-marginal regularizers

and information-theoretic quantities that will be discussed in the following sections. We note that, to facilitate the reading of our analysis, we write the CE and Dice losses in a non-standard way using summations over the ground-truth segmentation regions, rather than as functions of the labels. Also, while we provide the CE loss for all segmentation regions, we give Dice for a single region. This is to accommodate two variants of the Dice loss in the literature: in the binary case, Dice is typically used for the foreground region only [19]; in the multi-region case, it is commonly used over all the regions [26]. Finally, to simplify notation, we give all the loss functions for a single training image, without summations over all training samples (as this does not lead to any ambiguity, neither does it alter the analysis hereafter). In the training iterations, we use the mean values across all the training samples via standard mini-batch optimization.

## 2.1 Definition of label-marginal biases and penalty functions

In the following, we analyse the label-marginal biases inherent to CE and Dice losses, and show that the main difference between the two types of losses lies essentially in those label-marginal biases. To do so, we provide a constrained-optimization perspective of the losses: We define a label-marginal bias as a soft *penalty* function for the hard equality constraint  $\mathbf{p} = \mathbf{t}$ , where  $\mathbf{t}$  is a given (fixed) target distribution. Such a penalty encourages the predicted label-marginal  $\mathbf{p}$  to match a given target distribution  $\mathbf{t}$ . In the general context of constrained optimization, penalty functions are widely used [3]. In general, penalty methods replace equality constraints of the form  $\mathbf{p} = \mathbf{t}$  by adding a term  $g(\mathbf{p})$  to the main objective being minimized. Such a penalty function  $g$  increases when  $\mathbf{p}$  deviates from target  $\mathbf{t}$ . By definition, for the constraint  $\mathbf{p} = \mathbf{t}$ , with the domain of  $\mathbf{p}$  being probability simplex  $\Delta_K$ , a penalty  $g(\mathbf{p})$  is a continuous and differentiable function, which reaches its global minimum when the constraint is satisfied, i.e., it verifies:  $g(\mathbf{t}) \leq g(\mathbf{p}) \forall \mathbf{p} \in \Delta_K$ .

## 2.2 The link between Cross Entropy and Dice

To ease the discussion in what follows, we will start by analyzing the link between CE and the logarithmic Dice, along with the label-marginal bias of the latter (Proposition 1). Then, we discuss a bounding relationship between the different Dice variants. Finally, we will provide an information-theoretic analysis, which highlights the hidden label-marginal bias of CE (Proposition 2).

Let us consider the logarithmic Dice loss in the multi-class case. This loss decomposes (up to a constant) into two terms, a ground-truth matching term and a label-marginal bias:

$$-\sum_{k=1}^K \log(\text{Dice}_k) \stackrel{\text{c}}{=} \underbrace{-\sum_{k=1}^K \log \left( \frac{1}{|\Omega_k|} \sum_{i \in \Omega_k} p_{ik} \right)}_{\text{Ground-truth matching: DF}} + \underbrace{\sum_{k=1}^K \log(\hat{p}_k + \hat{y}_k)}_{\text{Label-marginal bias: DB}} \quad (1)$$

where  $\stackrel{c}{=}$  stands for equality up to an additive and/or non-negative multiplicative constant. The ground-truth matching term in Eq. (1) is a lower bound on the cross-entropy loss (CE) due to Jensen’s inequality and the convexity of function  $-\log(x)$ :  $\text{DF} \leq \text{CE}$ . Therefore, minimizing CE could be viewed as a proxy for minimizing term DF that appears in the logarithmic Dice. In fact, from a constrained-optimization perspective, DF and CE are very closely related and could be viewed as two different penalty functions enforcing the same equality constraints:  $p_{ik} = 1, \forall i \in \Omega_k, \forall k$ . Both DF and CE are monotonically decreasing functions of each softmax and reach their global minimum when these equality constraints are satisfied. Therefore, they encourage softmax predictions  $p_{ik}$  for each region  $\Omega_k$  to reach their target ground-truth values of 1. Of course, this does not mean that penalties CE and DF yield exactly the same results. The difference in the results that they may yield is due to the optimization technique (e.g., different gradient dynamics in the standard training of deep networks as the penalty functions have different forms).

### 2.3 The hidden label-marginal bias of Dice

The following proposition highlights how the label-marginal term DB in Eq. (1) encourages specific extremely imbalanced solutions.

**Proposition 1.** *Let  $\mathbf{t} = (\hat{t}_j)_{1 \leq j \leq K} \in \{0, 1\}^K$  denote the simplex vertex verifying:  $\hat{t}_j = 1$  when  $\hat{y}_j = \max_{1 \leq k \leq K} \hat{y}_k$  and  $\hat{t}_j = 0$  otherwise. For variables  $\mathbf{p} = (\hat{p}_k)_{1 \leq k \leq K}$  and fixed distribution  $\mathbf{y} = (\hat{y}_k)_{1 \leq k \leq K}$ , the label-marginal term in Eq. (1) reaches its minimum over the simplex at  $\mathbf{t}$ :*

$$\sum_{k=1}^K \log(\hat{t}_k + \hat{y}_k) \leq \sum_{k=1}^K \log(\hat{p}_k + \hat{y}_k) \quad \forall \mathbf{p} \in \Delta_K \quad (2)$$

*Proof.* The details of the proof are deferred to Appendix A.1. The main technical ingredient is based on Jensen’s inequality and the concavity of penalty DB with respect to simplex variables  $\mathbf{p}$ .

Inequality (2) means that the label-marginal term in Dice in Eq. (1) is a penalty function for constraint  $\mathbf{p} = \mathbf{t}$ , where  $\mathbf{t}$  is the simplex vertex given in Proposition 1. Therefore, it encourages extremely imbalanced segmentations, where a specific region includes all the pixels and the remaining regions are empty. All in all, the logarithmic Dice loss integrates a hidden label-marginal prior preferring extremely imbalanced segmentations, which is optimized jointly with a ground-truth matching term similar to CE. It is worth noting that, in the two-class (binary) segmentation case, Dice might be used for the foreground region only, as in the popular work in [19], for instance. Similarly to the multi-class case discussed above, a single Dice also decomposes into a ground-truth matching term and label-marginal penalty, with the latter encouraging extremely imbalanced binary segmentations. We provide more details for this case in Appendix B.

## 2.4 On the link between the different variants of Dice

The label-marginal analysis we discussed above is based on the standard logarithmic Dice loss. Here, we argue that both logarithmic and linear Dice are very closely related and, hence, the linear Dice also hides a class-imbalance bias. In fact, from a constrained-optimization perspective, the two losses could be viewed as different penalty functions for imposing constraints:  $\text{Dice}_k = 1 \forall k$ . Both functions  $-\log(x)$  and  $(1-x)$  are monotonically decreasing in  $[0, 1]$  and achieve their minimum in  $[0, 1]$  at  $x = 1$ . Furthermore, the logarithmic Dice is an upper bound on the linear one. This follows directly from:  $-\log(t) \geq 1-t \quad \forall t > 0$ . Of course, this does not mean that optimizing these two variants leads to exactly the same results. The differences in their results might be due to optimization (i.e., different gradient dynamics stemming from logarithmic and linear penalties).

## 2.5 The hidden label-marginal bias of CE

In the following, we give an information-theoretic perspective of CE, via a generative view of network predictions and a Monte-Carlo approximation of the entropy of the learned features given the labels. This highlights a hidden label-marginal bias of CE, which encourages the proportions of the predicted segmentation regions to match the ground-truth proportions.

**Proposition 2.** *Let  $\mathcal{F}$  and  $\mathcal{K}$  denote the random variables associated with the learned features and the labels, respectively, and  $\mathcal{H}(\mathcal{F}|\mathcal{K})$  the conditional entropy of learned features given the labels, estimated via Monte-Carlo :*

$$\mathcal{H}(\mathcal{F}|\mathcal{K}) \approx \sum_k^K y_k \mathcal{H}(\mathcal{F}|\mathcal{K} = k) \approx -\frac{1}{|\Omega|} \sum_k^K \sum_{i \in \Omega_k} \log(\mathbb{P}(\mathbf{f}_i^\theta | k)) \quad (3)$$

where  $\mathcal{H}(\mathcal{F}|\mathcal{K} = k)$  is the empirical estimate of the conditional entropy of features given a specific class  $k$  (expression in Table 1) and  $\mathbb{P}(\mathbf{f}_i^\theta | k)$  denotes the probability of the learned features given class  $k$ . We have the following generative view of CE:

$$\text{CE} \stackrel{\text{c}}{=} \underbrace{\mathcal{H}(\mathcal{F}|\mathcal{K})}_{\text{Ground-truth matching}} + \underbrace{\mathcal{D}_{\text{KL}}(\mathbf{y}||\mathbf{p})}_{\text{Label-marginal bias}} \quad (4)$$

The detailed proof is deferred to Appendix A.2. The approximation of  $\mathcal{H}(\mathcal{F}|\mathcal{K} = k)$  in the second line of Eq. (3) is based on the well-known Monte-Carlo estimation [10,23]. Then the relationship in Eq. (4) follows from Eq. (3), after some manipulations, using Bayes rule  $\mathbb{P}(\mathbf{f}_i^\theta | k) \propto \frac{p_{ik}}{\hat{p}_k}$  and  $\sum_{i \in \Omega_k} \log(\hat{p}_k) = |\Omega_k| \log(\hat{p}_k)$ .

This information-theoretic view of CE shows that the latter has an implicit (hidden) label-marginal bias towards the ground-truth region proportions (the KL term). This bias competes with the entropy term, which encourages low uncertainty (variations) within each ground-truth segmentation region  $\Omega_k$ . The

entropy term could be viewed as a ground-truth matching term: it reaches its global minima when the feature embedding is constant within each region. If used alone, the entropy term may lead to trivial imbalanced solutions. The label-marginal KL term avoids such trivial solutions by matching the ground-truth class proportions. Note that there is no mechanism in CE to control the relative contributions of those two competing terms as they are implicit in CE.

## 2.6 Our solution

Our analysis shows that Dice, CE and their combinations, e.g.,  $\text{CE} - \log(\text{Dice})$ , are closely related and enforce two types of competing constraints : ground-truth matching and label-marginal constraints. However, there is no clear consensus in the literature as to which loss is better, with the performances of each varying across data sets and applications. This variability in performances could be explained by two fundamental factors:

- **The difference in the label-marginal prior.** The label-marginal priors are different as Dice has an intrinsic bias preferring very small regions, while CE encourages the right (ground-truth) region proportions. This might explain the wide experimental evidence in the medical imaging literature, where using or adding Dice losses brings improvements for imbalanced segmentation with extremely small regions.

- **Weighting the contribution of the bias term.** Our analysis suggests that CE should be preferred over Dice in all cases and applications (both balanced/imbalanced segmentation, or segmentation problems with high variability in region proportions) as it promotes the right label-marginal distribution. While this seems to be widely the case in natural image segmentation, where Dice is uncommon, the extensive experimental evidence in the medical-image segmentation literature suggests otherwise, especially in extremely imbalanced problems. We argue that this is due to the relative contribution of the label-marginal term in the overall objective. Controlling such label-marginal contribution is very important in imbalanced problems. In particular, it mitigates the difficulty that the ground-truth matching terms differ by several orders of magnitude across regions, as in CE, which causes large-region terms to completely dominate small-region ones. This analysis also resonates with the fact that combo losses such

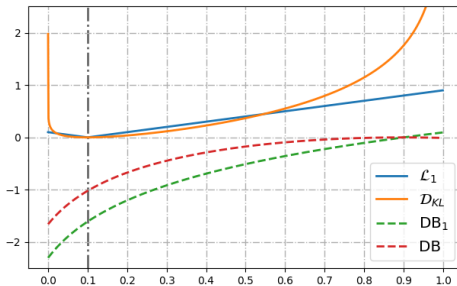


**Fig. 2. Different label-marginal biases.**

The ground-truth foreground region proportion is set to 0.1. The expression of penalty  $\text{DB}_1$  is provided in Appendix B, and corresponds to the two-class (binary) variant of Dice, where the loss is used over the foreground region only. Penalty  $\mathcal{L}_1$  presents better gradient dynamics at the vicinity of label marginal  $\hat{p}_1 = 0$ . Best seen in color.



as  $\text{CE} - \lambda \log(\text{Dice})$  perform very competitively in imbalanced segmentation, as shown by [26,22], among several other recent works. In this case, controlling the relative contribution of each of these terms indirectly controls the weight of the label-marginal bias. Note that such control is not possible when using CE alone or Dice alone, as the label-marginal biases in these losses are hidden (implicit).

We propose a principled and simple solution, which enables to control explicitly the label-marginal bias, via regularization losses that encourage the correct class proportions and are used in conjunction with CE :

$$\text{CE} + \lambda \mathcal{R}(\mathbf{y}; \mathbf{p}) \quad (5)$$

Our label-marginal regularizers increase the contribution of the minority classes in imbalanced problems, but, unlike Dice, do not lose adaptability to problems with various class proportions. Our extensive experiments and ablation studies over different losses and applications demonstrate the effectiveness of our explicit label-marginal regularizers. We investigate different forms of regularization, including the  $\mathcal{L}_1$  norm, i.e.,  $\mathcal{R}(\mathbf{y}; \mathbf{p}) = \mathcal{L}_1(\mathbf{y}, \mathbf{p})$ , and the KL divergence, i.e.,  $\mathcal{R}(\mathbf{y}; \mathbf{p}) = \mathcal{D}_{\text{KL}}(\mathbf{y}||\mathbf{p})$ ; see Table 1 for the expressions of  $\mathcal{D}_{\text{KL}}$  and  $\mathcal{L}_1$ . In Fig. 2, we depict our different regularizers as functions of the label-marginal distribution for a binary-segmentation case, with the foreground-region proportion set to 0.1, along with the bias terms in Dice. While our  $\mathcal{D}_{\text{KL}}$  and  $\mathcal{L}_1$  regularizers may deliver comparable performances (see the experimental section),  $\mathcal{L}_1$  might be a better option for extremely imbalanced segmentations, due to its gradient properties and stability at the vicinity of 0, i.e., when the label-marginal probability  $\hat{p}_1$  is close to 0. Notice that, at the vicinity of zero, both first and second derivatives of the regularizer are *unbounded* for  $\mathcal{D}_{\text{KL}}$ , but *bounded* and *constant* for  $\mathcal{L}_1$ . Our experiments on imbalanced medical image segmentation confirm the effectiveness of the  $\mathcal{L}_1$  regularizer.

### 3 Experiments

**Datasets.** We validate the proposed method on four different segmentation benchmarks, including 2D and 3D medical image applications, and natural image segmentation. Here, we present the description of all the datasets, as well as the corresponding implementation details.

- **Retinal Lesions**[25] is a large collection of color fundus images. A panel of 45 experienced ophthalmologist was formed to label this dataset and each image was assigned to at least three annotators to get trustworthy pixel-level lesions annotations[25]. In our experiments, we employ its public version<sup>4</sup>, consisting of 1,593 samples. To cover the widely used binary setting of Dice-related losses, we first conduct our experiments in the binary scenario (segment the lesion region versus background). The dataset is randomly divided into training (70%), validation (10%) and test (20%) set, whose images are resized to  $512 \times 512$ . The standard encoder-decoder segmentation architecture is used, with difference

<sup>4</sup> <https://github.com/WeiQijie/retinal-lesions>

settings of encoder (Res34 and Res50[7]) and decoder (FPN[15] and Unet[20]), whose implementations are publicly available<sup>5</sup>. We train the model during 60 epochs with batch size set to 8 via Adam optimizer. The initial learning rate is set to  $1e-4$  and halved if the loss on the validation set does not decrease within 5 epochs.

- **Pancreas** and **Liver** datasets are provided in the Medical Segmentation Decathlon[1]. Pancreas includes 281 portal-venous phase 3D CT scans of patients undergoing resection of pancreatic masses. The segmenting targets consists of two categories, i.e., pancreas and tumor. For Liver, it consists of 201 contrast-enhanced CT cases. The corresponding regions of interest are the segmentation of the liver and tumors inside the liver. On both datasets, the unbalance between the large (background), medium (pancreas or liver) and small (tumor) structures makes them significantly challenging. We use nnU-Net[8] as the backbone architecture. The dataset is randomly split into 80% for training and 20% for testing. SGD optimizer is used with an initial learning rate of 0.01, which is decayed throughout the training via polynomial strategy to linearly scale down to 0. All networks are trained for 1k epochs with a batch size of 2. Note that the hyper-parameters for the loss functions are set as the best values obtained on the Retinal Lesions dataset.

- **Cityscapes**[5] is a large-scale natural scene dataset with high quality pixel-level annotations of 5k images across 19 categories, containing both stuff and objects with high variation in the class proportions distribution. We use the official data split, which contains 2,975 samples for training, 500 samples for validation and 1,512 samples for testing. All the input images are resized to  $512 \times 1024$  for training, and  $1024 \times 2048$  for testing. The main setting is adopted from the state-of-the-art library<sup>6</sup>. Specifically, SGD optimizer is used for training, with the initial learning rate set to 0.01 and a batch size of 8. During the 100 training epochs, we use an iteration-wise polynomial strategy to linearly scale the learning rate down to a minimum of  $1e-4$ .

**Losses.** We evaluate the proposed loss function in Eq. (5) with two different penalty terms, i.e., Ours( $\mathcal{D}_{KL}$ ) and Ours( $\mathcal{L}_1$ ). In our implementation, we use a modified soft-max function with a temperature parameter when computing the predicted region proportion, as this enables a better estimate of the actual region proportion (refer to Appendix C for details). We compare our results with the following relevant losses : CE, Focal loss (FL), Dice related losses, i.e., linear Dice (1-Dice), logarithmic Dice ( $-\log(\text{Dice})$ ) and generalized Dice (GDice), and the composite losses integrating CE with linear Dice (DiceCE) or logarithmic Dice (LogDiceCE); a recent detailed survey of these losses could be found in [18].

**Evaluation metrics.** On Retinal Lesions, we use standard metrics in medical image segmentation: Dice Similarity Coefficient (DSC) and the modified Hausdorff Distance (HD-95), which represents the 95th percentile of the symmetric Hausdorff Distance between the binary objects in two images. On Pancreas and Liver, we follow the official measures in the Medical Segmentation Decathlon to

<sup>5</sup> [https://github.com/qubvel/segmentation\\_models.pytorch](https://github.com/qubvel/segmentation_models.pytorch)

<sup>6</sup> <https://github.com/open-mmlab/mmssegmentation>

**Table 2. Quantitative evaluations of different losses on Retinal Lesions.** Average DSC and HD95 values (and standard deviation over three independent runs) achieved on the test set are reported. Note that  $\text{Dice}_1$  is implemented for all the Dice related losses for the binary setting on this dataset, and DiceBias here refers to label-marginal bias for the binary Dice (details can be found in Appendix B).

Loss	Res34-FPN		Res34-Unet		Res50-FPN		Res50-Unet	
	DSC (%)	HD-95 (mm)	DSC(%)	HD-95 (mm)	DSC(%)	HD-95 (mm)	DSC(%)	HD-95 (mm)
CE	51.4 (0.1)	85.5 (2.0)	52.4 (0.5)	85.5 (3.7)	52.7 (0.1)	80.6 (2.6)	52.7 (0.3)	84.3 (4.1)
FL	51.2 (0.2)	84.4 (4.9)	51.2 (0.8)	88.6 (4.9)	52.9 (0.4)	80.9 (2.8)	51.8 (0.6)	84.4 (1.9)
$1 - \text{Dice}_1$	52.0 (0.7)	84.8 (3.3)	52.3 (0.7)	89.2 (2.4)	52.0 (0.7)	82.2 (4.0)	53.2 (0.1)	81.9 (4.0)
$-\log(\text{Dice}_1)$	51.7 (0.9)	86.0 (4.4)	52.7 (0.5)	85.8 (0.2)	52.0 (1.0)	81.7 (3.6)	53.5 (0.5)	82.2 (2.8)
GDice	51.9 (0.7)	86.7 (2.7)	52.4 (0.5)	90.0 (1.3)	53.4 (0.3)	80.8 (2.4)	53.7 (0.4)	86.8 (3.2)
DiceCE	51.6 (0.7)	85.7 (3.0)	52.1 (0.1)	87.9 (2.7)	53.2 (0.5)	80.9 (1.7)	53.0 (0.9)	82.3 (2.7)
LogDiceCE	52.2 (0.5)	81.6 (6.7)	52.6 (0.4)	84.1 (2.4)	53.2 (0.5)	78.4 (2.1)	53.4 (0.3)	82.6 (2.1)
DiceBiasCE	51.7 (0.9)	82.7 (1.7)	51.8 (0.2)	86.1 (1.8)	53.4 (0.4)	78.7 (1.2)	53.2 (0.1)	83.0 (0.5)
Ours( $\mathcal{D}_{\text{KL}}$ )	52.7 (0.3)	83.3 (2.4)	52.8 (0.3)	82.7 (2.4)	53.8 (0.1)	77.1 (1.8)	53.8 (0.4)	80.2 (1.3)
Ours( $\mathcal{L}_1$ )	<b>52.8 (0.3)</b>	<b>80.7 (2.5)</b>	<b>53.1 (0.2)</b>	<b>81.2 (2.8)</b>	<b>54.5 (0.2)</b>	<b>75.0 (2.0)</b>	<b>54.3 (0.2)</b>	<b>77.0 (1.5)</b>

report DSC and NSD (normalized surface distance), where NSD is a boundary-based metric. On Cityscapes, we resort to the standard Intersection-Over-Union (IoU) score, which is widely employed in the natural image scenario.

### 3.1 Results

**Results on Retinal Lesions.** Table 2 reports the quantitative comparison between the proposed loss and the related methods. Regardless of the networks and metrics, Ours( $\mathcal{L}_1$ ) consistently achieve the best performance. On Res50-FPN, for instance, compared to CE, our best model, i.e.,  $\mathcal{L}_1$  as the label-marginal regularizer, brings nearly 2.0% improvement in terms of DSC and 5% in terms of HD-95. It is noteworthy to mention that while DSC is more sensitive to the internal filling of the target region, the HD-95 is more sensitive to the segmentation boundary. Thus, the more significant improvement on HD-95 indicate that the proposed loss is more effective to predict better boundaries than existing losses. Regarding the robustness, the proposed losses present a more stable performance across different runs and backbones, which is reflected in their lower variances. This can be explained by their better adaptability to different target sizes and better gradient dynamics at the vicinity of label marginal  $\hat{p}_k = 0$  (as shown in Fig. 2). Another interesting finding is that, by combining CE with the bias term of Dice (DiceBiasCE), we obtain results close to the combo losses (DiceCE and LogDiceCE). This validates our theoretical insight that the fundamental difference between CE and Dice lies in their distinct hidden biases.

**Ablation study on the balancing weight.** We study the impact of the balancing weight  $\lambda$  in the proposed loss in Eq. (5), as well as the balancing weight in other composite losses like DiceCE and LogDiceCE, presented in Fig. 3. It is empirically found that the best  $\lambda$  values for different penalty terms are : 1.0 for Ours( $\mathcal{L}_1$ ), 0.1 for Ours( $\mathcal{D}_{\text{KL}}$ ), and 0.1 for DiceCE and LogDiceCE. From the curves, we can notice that  $\mathcal{L}_1$  is a better choice than KL divergence because of its better stability. This may relate to its gradient properties and stability at the vicinity of 0 as shown in Fig. 2. Thus, we can use a relatively larger weighting

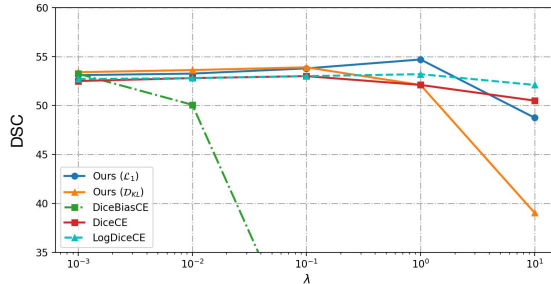


**Fig. 3.** The performances of different composite losses on the test set of Retinal Lesions with different values of the balancing weight  $\lambda$ . The network here is fixed to Res50-FPN.

value in Ours( $\mathcal{L}_1$ ). For the loss integrating CE with the Dice bias term, i.e., Dice-BiasCE, we demonstrate that it can yield performances similar to DiceCE and LogDiceCE, but it drops significantly with high weighting values ( $\lambda \geq 0.1$ ). This might be due to its gradient characteristics. Comparing to the widely suggested composite loss of CE and Dice, our method deliver better performance with the same hyper-parameter budget. Note, we use the best empirical values of  $\lambda$  found on Retinal Lesions for the experiments on 3D medical image segmentation (Pancreas and Liver) and Cityscapes.

**Table 3. Results on 3D medical image segmentation.** On both datasets, i.e., Pancreas and Liver, we report DSC and NSD scores achieved on the test set.

Loss	Pancreas						Liver					
	DSC (%)			NSD (%)			DSC (%)			NSD (%)		
	pan.	tum.	mean	pan.	tum.	mean	liv.	tum.	mean	liv.	tum.	mean
CE	81.8	41.6	61.7	59.9	26.5	43.2	<b>96.6</b>	60.2	78.4	69.4	40.9	55.1
Focal loss	81.6	42.4	62.0	59.4	28.3	43.9	<b>96.6</b>	63.7	80.1	69.5	42.7	56.1
1 – Dice	78.9	43.3	61.1	54.5	26.2	40.4	96.4	65.0	80.7	67.7	45.0	56.4
–log(Dice)	81.9	42.2	62.1	61.0	27.3	44.1	96.2	62.9	79.6	67.8	44.1	55.9
DiceCE	81.8	43.0	62.4	59.9	28.0	44.0	96.5	65.9	81.2	68.2	45.3	56.7
LogDiceCE	81.4	43.2	62.3	59.9	27.9	43.9	<b>96.6</b>	63.7	80.1	<b>69.6</b>	44.6	57.2
Ours ( $\mathcal{D}_{KL}$ )	82.1	46.2	64.1	60.3	30.4	45.3	96.5	62.0	79.3	69.4	40.8	55.1
<b>Ours (<math>\mathcal{L}_1</math>)</b>	<b>82.2</b>	<b>47.6</b>	<b>64.9</b>	<b>61.1</b>	<b>32.0</b>	<b>46.6</b>	<b>96.6</b>	<b>66.5</b>	<b>81.6</b>	69.1	<b>46.7</b>	<b>57.9</b>

**Results on 3D medical image segmentation.** We now investigate the performance on two 3D medical image segmentation benchmarks, i.e., Pancreas and Liver, whose results are reported in Table 3. It is observed that the proposed approach leads to the best performance in most cases, which is consistent with the empirical results on 2D retinal images. In particular, the improvement on the more challenging class (small structured tumor) are significant. Compared to CE, for instance, our best model increases the DSC of tumor on Pancreas and Liver by 4.6 and 6.6 percent respectively. Our theoretic analysis is further validated that the Dice related losses (linear and logarithmic Dice) can bring improvement for the imbalanced categories, while the improvement of the proposed method is

more stable and significant under different conditions and metrics. Note that the best performance of our method on the boundary metric, NSD, indicates that our method yields more accurate boundaries, probably due to the encourage of predicting right proportion.

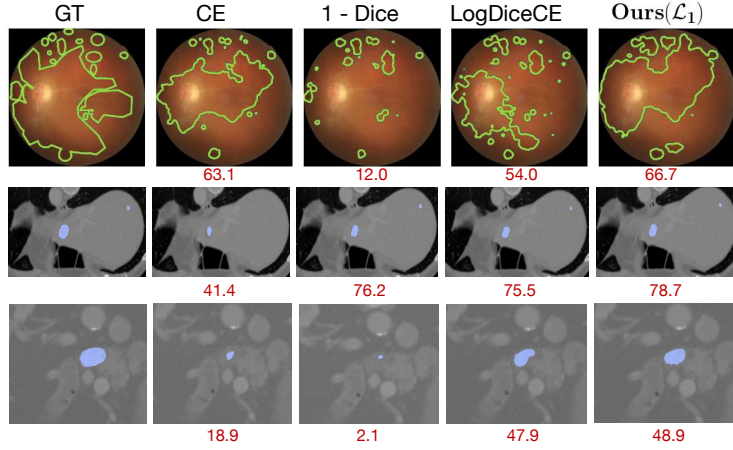


**Fig. 4. Visual results on the medical imaging.** Examples are from Retinal Lesions (Top), Liver (Middle) and Pancreas (Bottom). The ground-truth is provided in the first column. At the bottom of each prediction, we indicate the corresponding DSC score.

**Qualitative results.** Some visualized examples from medical datasets are presented in Fig. 4. We can observe that the model trained with Dice variants (*third* and *fourth* column) tends to under-segment large and medium target regions (Top, Bottom), while CE could miss some small structures (Middle). In contrast, the proposed solution enables a better trade-off between finding small regions, reducing the number of false positives and matching the size of the larger targets. Furthermore, one can notice that our loss yields better consistencies with the target region proportions than the others.

**Results on Cityscapes.** Table 4 reports the comparative per-class IoU and mean IoU (mIoU) on the validation set of Cityscapes with two network architectures. First, we can observe that in this multi-class dataset, regardless of the network, the proposed learning objectives outperform all the evaluated losses in terms of mIoU. Then, by investigating the relationship between region proportion, mRegProp (second row in Table 4), and the corresponding segmentation performance across small region classes, we can observe that Dice-related losses have a hidden label-marginal bias towards extremely imbalanced solutions, preferring small structures. In particular, the linear Dice often obtains the highest IoU for the smallest structures. This bias comes at the cost of less flexibility when dealing with arbitrary class proportions, which is reflected in its poor mIoU (*right column*). Quantitative evaluation on the Cityscapes test set is reported in Table 5. The observations in this table are consistent with those on the validation set,

**Table 4. Results on Cityscapes validation set.** (Top: *Res50-FPN*, Bottom: *Res101-FPN*) The second row indicates the average region proportion (mRegProp) for each class. mIoU denotes the mean IoU score over all classes.

	road	swalk	build.	wall	fence	pole	tlight	sign	veg.	terrain	sky	person	rider	car	truck	bus	train	mbike	bike	mIoU
mRegProp(%)	32.6	5.4	20.2	0.6	0.8	1.1	0.2	0.5	14.1	1.0	3.6	1.1	0.1	6.2	0.2	0.2	0.2	0.1	0.4	
CE	97.2	<b>80.6</b>	90.0	38.2	51.3	55.7	60.5	72.2	<b>91.0</b>	58.6	92.3	75.6	48.5	92.5	50.5	67.7	56.3	50.2	71.6	68.5
Focal loss	97.1	78.8	89.5	37.9	48.9	51.8	56.9	67.6	90.6	56.9	92.6	73.1	42.8	92.0	47.5	57.5	46.1	49.2	68.4	65.5
1 – Dice	95.9	77.6	87.7	<b>41.1</b>	47.6	56.0	<b>66.2</b>	<b>74.8</b>	90.0	59.6	93.1	<b>77.3</b>	<b>55.8</b>	91.1	10.0	63.9	34.6	53.6	<b>73.6</b>	65.8
– log Dice	94.0	70.8	85.6	33.2	39.1	50.6	62.2	69.6	88.4	52.1	88.1	74.2	50.7	89.2	34.8	55.3	31.7	48.0	70.7	62.5
DiceCE	97.0	79.7	89.7	43.4	48.6	55.4	61.4	71.7	91.0	57.4	92.6	75.5	48.6	92.5	44.4	63.6	52.1	51.8	71.5	67.8
LogDiceCE	96.9	78.6	89.8	40.4	48.3	<b>57.1</b>	65.4	74.6	90.7	57.2	92.5	77.0	52.7	92.4	47.9	65.0	50.6	51.4	72.6	68.5
Ours ( $\mathcal{D}_{KL}$ )	97.2	79.6	90.0	39.6	51.2	54.8	60.3	71.5	<b>91.0</b>	<b>59.7</b>	92.9	75.2	49.0	92.7	<b>55.6</b>	<b>72.5</b>	<b>65.6</b>	51.3	70.9	69.5
<b>Ours (<math>\mathcal{L}_1</math>)</b>	<b>97.4</b>	80.2	<b>90.1</b>	37.9	<b>51.9</b>	55.7	61.0	72.1	<b>91.0</b>	58.9	<b>93.5</b>	75.7	49.8	<b>92.8</b>	54.9	70.2	62.8	<b>54.0</b>	71.6	<b>69.6</b>
CE	<b>97.8</b>	82.4	91.0	46.5	55.3	57.2	62.6	72.3	91.5	60.7	<b>94.2</b>	76.1	50.7	93.6	68.4	77.2	64.8	54.9	72.6	72.1
Focal loss	97.7	81.9	90.8	<b>48.2</b>	54.1	54.4	59.0	69.4	91.0	60.2	93.7	74.7	47.8	93.0	59.3	67.3	51.9	52.1	70.5	69.3
1 – Dice	96.4	79.6	88.1	0.0	50.6	<b>58.4</b>	<b>69.0</b>	<b>76.0</b>	90.2	60.4	93.7	<b>78.7</b>	<b>60.0</b>	91.4	35.1	0.0	26.8	0.0	<b>74.5</b>	59.4
– log Dice	95.2	73.9	86.4	31.5	39.2	52.4	63.3	70.4	88.6	53.0	92.2	74.6	52.1	89.4	37.1	57.3	31.1	42.7	71.5	63.3
DiceCE	97.6	81.8	90.9	46.7	52.8	59.5	68.5	76.8	91.3	59.5	94.0	78.3	57.1	93.5	56.9	72.1	56.6	53.2	74.5	71.7
LogDiceCE	97.2	79.9	90.2	42.5	52.2	57.6	66.7	74.8	90.9	59.6	93.7	77.7	57.4	92.9	56.4	72.1	58.9	54.2	74.0	71.0
Ours ( $\mathcal{D}_{KL}$ )	<b>97.8</b>	82.6	91.1	45.4	<b>56.8</b>	57.4	63.4	72.5	91.5	<b>61.3</b>	94.0	76.7	52.4	93.7	69.2	78.3	64.5	57.1	72.8	72.6
<b>Ours (<math>\mathcal{L}_1</math>)</b>	<b>97.8</b>	<b>82.9</b>	<b>91.2</b>	48.0	<b>56.8</b>	57.7	63.8	72.7	<b>91.6</b>	61.2	93.8	76.9	52.8	<b>93.8</b>	<b>77.1</b>	<b>80.0</b>	<b>67.1</b>	<b>57.2</b>	73.1	<b>73.4</b>

that our method achieves better results on both architectures. For the per-class scores on the test set, please refer to Appendix D.

It is noteworthy to highlight that both linear Dice and logarithmic Dice perform relatively poorly on Cityscapes, on average, empirically showing why Dice is rarely adopted in natural image segmentation tasks. As we mentioned earlier, this might be due to its inherent label-marginal bias, which is inappropriate for segmenting regions with arbitrary class proportions. Furthermore, our simple solution beats CE and Dice-related losses, regardless of the backbone. These empirical observations suggest that the proposed formulation in Eq. (5) results in better region-proportion guidance and training stability than existing segmentation losses.

**Table 5. mIoU on Cityscapes test set.**

Loss	Res50-FPN	Res101-FPN
CE	67.0	69.6
Focal loss	64.5	66.8
1 – Dice	63.7	59.4
– log(Dice)	59.8	62.6
DiceCE	66.6	69.7
LogDiceCE	67.1	69.6
Ours ( $\mathcal{D}_{KL}$ )	<b>68.4</b>	<b>70.1</b>
<b>Ours (<math>\mathcal{L}_1</math>)</b>	<b>68.4</b>	<b>70.1</b>

## 4 Conclusion

We provided a detailed theoretical analysis of the two most popular semantic segmentation losses, i.e., Cross-entropy and Dice, which revealed non-obvious bounding relationships and hidden label-marginal biases, suggesting that CE is a better option in general. Then, we showed how both loss functions could be written under a common formulation, containing a ground-truth matching term and a label-marginal bias. The implicit bias in Dice prefers small regions, improving its performance in highly imbalanced conditions, as in medical-imaging applications. The bias hidden in CE encourages the ground-truth region proportion, which makes it a generally better option in complex scenarios with diverse

class proportions. Furthermore, we proposed a principled solution, which enables to control the label-marginal bias via  $\mathcal{L}_1$  and KL penalties that encourage the target class proportions, while improving training stability. Our flexible formulation enables the minority classes to have better influence on training, without losing adaptability to medium-to-large regions. Extensive experiments on four benchmarks, covering 2D and 3D medical imaging applications, and natural scenario, validate the theoretical analysis in this paper, as well as the effectiveness of the presented solution.

## References

1. Antonelli, M., Reinke, A., Bakas, S., Farahani, K., AnnetteKopp-Schneider, Landman, B.A., Litjens, G., Menze, B., Ronneberger, O., Summers, R.M., van Ginneken, B., Bilello, M., Bilic, P., Christ, P.F., Do, R.K.G., Gollub, M.J., Heckers, S.H., Huisman, H., Jarnagin, W.R., McHugo, M.K., Napel, S., Pernicka, J.S.G., Rhode, K., Tobon-Gomez, C., Vorontsov, E., Huisman, H., Meakin, J.A., Ourselin, S., Wiesenfarth, M., Arbelaez, P., Bae, B., Chen, S., Daza, L., Feng, J., He, B., Isensee, F., Ji, Y., Jia, F., Kim, N., Kim, I., Merhof, D., Pai, A., Park, B., Perslev, M., Rezaiifar, R., Rippel, O., Sarasua, I., Shen, W., Son, J., Wachinger, C., Wang, L., Wang, Y., Xia, Y., Xu, D., Xu, Z., Zheng, Y., Simpson, A.L., Maier-Hein, L., Cardoso, M.J.: The medical segmentation decathlon. arXiv preprint arXiv:2106.05735 (2021)
2. Bao, H., Dong, L., Wei, F.: BEiT: BERT pre-training of image transformers. arXiv preprint arXiv:2106.08254 (2021)
3. Bertsekas, D.: Nonlinear Programming. Athena Scientific, Belmont, MA (1995)
4. Chen, L.C., Zhu, Y., Papandreou, G., Schroff, F., Adam, H.: Encoder-decoder with atrous separable convolution for semantic image segmentation. In: ECCV (2018)
5. Cordts, M., Omran, M., Ramos, S., Rehfeld, T., Enzweiler, M., Benenson, R., Franke, U., Roth, S., Schiele, B.: The cityscapes dataset for semantic urban scene understanding. In: CVPR (2016)
6. Dolz, J., Desrosiers, C., Ben Ayed, I.: 3d fully convolutional networks for subcortical segmentation in mri: A large-scale study. *NeuroImage* **170**, 456–470 (2018)
7. He, K., Zhang, X., Ren, S., Sun, J.: Deep residual learning for image recognition. In: CVPR (2016)
8. Isensee, F., Jaeger, P.F., Kohl, S.A., Petersen, J., Maier-Hein, K.H.: nnu-net: a self-configuring method for deep learning-based biomedical image segmentation. *Nature methods* **18**(2), 203–211 (2021)
9. Jha, D., Riegler, M.A., Johansen, D., Halvorsen, P., Johansen, H.D.: Doubleu-net: A deep convolutional neural network for medical image segmentation. In: CBMS (2020)
10. Kearns, M.J., Mansour, Y., Ng, A.Y.: An information-theoretic analysis of hard and soft assignment methods for clustering. In: UAI (1997)
11. Kervadec, H., Bahig, H., Letourneau-Guillon, L., Dolz, J., Ayed, I.B.: Beyond pixel-wise supervision for segmentation: A few global shape descriptors might be surprisingly good! In: MIDL (2021)
12. Kervadec, H., Bouchtiba, J., Desrosiers, C., Granger, E., Dolz, J., Ben Ayed, I.: Boundary loss for highly unbalanced segmentation. *Medical Image Analysis* **67**, 101851 (2021)

13. Kim, J., III, J.W.F., Yezzi, A.J., Çetin, M., Willsky, A.S.: A nonparametric statistical method for image segmentation using information theory and curve evolution. *IEEE Transactions on Image Processing* **14**(10), 1486–1502 (2005)
14. Kirillov, A., He, K., Girshick, R., Rother, C., Dollar, P.: Panoptic segmentation. In: *CVPR* (June 2019)
15. Lin, T., Dollár, P., Girshick, R., He, K., Hariharan, B., Belongie, S.: Feature pyramid networks for object detection. In: *CVPR* (2017)
16. Lin, T., Goyal, P., Girshick, R.B., He, K., Dollár, P.: Focal loss for dense object detection. In: *ICCV* (2017)
17. Litjens, G., Kooi, T., Bejnordi, B.E., Setio, A.A.A., Ciompi, F., Ghafoorian, M., van der Laak, J.A.W.M., van Ginneken, B., Sánchez, C.I.: A survey on deep learning in medical image analysis. *Medical Image Analysis* **42**, 60–88 (2017)
18. Ma, J., Chen, J., Ng, M., Huang, R., Li, Y., Li, C., Yang, X., Martel, A.L.: Loss odyssey in medical image segmentation. *Medical Image Analysis* **71**, 102035 (2021)
19. Milletari, F., Navab, N., Ahmadi, S.: V-net: Fully convolutional neural networks for volumetric medical image segmentation. In: *3DV* (2016)
20. Ronneberger, O., Fischer, P., Brox, T.: U-net: Convolutional networks for biomedical image segmentation. In: *MICCAI* (2015)
21. Sudre, C., Li, W., Vercauteren, T., Ourselin, S., Cardoso, M.J.: Generalised dice overlap as a deep learning loss function for highly unbalanced segmentations. In: *DLMIA/ML-CDS@MICCAI* (2017)
22. Taghanaki, S.A., Zheng, Y., Zhou, S.K., Georgescu, B., Sharma, P., Xu, D., Comaniciu, D., Hamarneh, G.: Combo loss: Handling input and output imbalance in multi-organ segmentation. *Computerized Medical Imaging and Graphics* **75**, 24–33 (2019)
23. Tang, M., Marin, D., Ayed, I.B., Boykov, Y.: Kernel cuts: Kernel and spectral clustering meet regularization. *International Journal of Computer Vision* **127**(5), 477–511 (2019)
24. Tao, A., Sapra, K., Catanzaro, B.: Hierarchical multi-scale attention for semantic segmentation. *arXiv preprint arXiv:2005.10821* (2020)
25. Wei, Q., Li, X., Yu, W., Zhang, X., Zhang, Y., Hu, B., Mo, B., Gong, D., Chen, N., Ding, D., Chen, Y.: Learn to segment retinal lesions and beyond. In: *ICPR* (2020)
26. Wong, K.C.L., Moradi, M., Tang, H., Syeda-Mahmood, T.F.: 3d segmentation with exponential logarithmic loss for highly unbalanced object sizes. In: *MICCAI* (2018)
27. Wu, Z., Shen, C., van den Hengel, A.: Bridging category-level and instance-level semantic image segmentation. *arXiv preprint arXiv:1605.06885* (2016)
28. Yeung, M., Sala, E., Schönlieb, C., Rundo, L.: A mixed focal loss function for handling class imbalanced medical image segmentation. *arXiv preprint arXiv:2102.04525* (2021)
29. Yuan, Y., Chen, X., Wang, J.: Object-contextual representations for semantic segmentation. In: *ECCV* (2020)
30. Zhao, H., Shi, J., Qi, X., Wang, X., Jia, J.: Pyramid scene parsing network. In: *CVPR* (2017)
31. Zhao, H., Zhang, Y., Liu, S., Shi, J., Change Loy, C., Lin, D., Jia, J.: Psanet: Point-wise spatial attention network for scene parsing. In: *ECCV* (2018)



## A Proofs

### A.1 Proposition 1

*Proof.* Let us write the label-marginal bias term in the logarithmic Dice as a vector-valued function of probability simplex vector  $\mathbf{p}$ :

$$g(\mathbf{p}) = \mathbf{1}_K^\top \log(\mathbf{p} + \mathbf{y}) \quad \text{for} \quad \mathbf{p} = (\hat{p}_k)_{1 \leq k \leq K} \in \Delta_K \quad (6)$$

where symbol  $\top$  denotes transpose and  $\mathbf{1}_K$  is the  $K$ -dimensional vector of ones. Function  $g$  is concave because its Hessian is a negative semi-definite matrix: The Hessian of  $g$  is a diagonal matrix whose diagonal elements are given by  $-\frac{1}{\hat{p}_k^2}$  and, hence, are all non-positive. Therefore, using Jensen's inequality and the fact that  $\mathbf{p}$  is within the simplex, we have the following lower bound on penalty  $g$  in Eq. (6):

$$g(\mathbf{p}) = g\left(\sum_{k=1}^K \hat{p}_k \mathbf{e}_k\right) \geq \sum_{k=1}^K \hat{p}_k g(\mathbf{e}_k) \quad (7)$$

where  $\mathbf{e}_k \in \{0, 1\}^K$  denote the  $k$ -th vertex of the simplex: the  $k$ -th component of  $\mathbf{e}_k$  is equal to 1 while the other components are all equal to 0. Now, recall the definition of simplex vector  $\mathbf{t} = (\hat{t}_j)_{1 \leq j \leq K}$ :  $\hat{t}_j = 1$  when  $\hat{y}_j = \max_{1 \leq k \leq K} \hat{y}_k$  and  $\hat{t}_j = 0$  otherwise. Given this definition, one could easily verify the following fact:

$$g(\mathbf{e}_k) \geq g(\mathbf{t}) \quad \forall k \quad (8)$$

To see this, let  $j$  denotes the integer verifying  $\hat{y}_j = \max_{1 \leq k \leq K} \hat{y}_k$  and let  $k \neq j$ . Then, we have:

$$g(\mathbf{e}_k) - g(\mathbf{t}) = \log\left(1 + \frac{1}{\hat{y}_k}\right) - \log\left(1 + \frac{1}{\hat{y}_j}\right) \geq 0. \quad (9)$$

This is due to the fact that function  $\log\left(1 + \frac{1}{x}\right)$  is monotonically decreasing in  $[0, 1]$  and  $\hat{y}_k \leq \hat{y}_j$ . Now, combining inequalities (7) and (8), and using the fact that  $\sum_{k=1}^K \hat{p}_k = 1$ , we obtain:

$$g(\mathbf{p}) \geq g(\mathbf{t}) \quad (10)$$

### A.2 Proposition 2

*Proof.* Considering a generative view of the prediction model, random variable  $\mathcal{F}$  associated with the learned features is continuous, while the random variable describing the labels, *i.e.*,  $\mathcal{K}$ , takes its possible values in a finite set  $\{1, \dots, K\}$ . Then, the marginal distribution of the labels could be empirically estimated by the GT proportion of each segmentation region (as listed in Table 1) [13] :

$$\mathbb{P}(\mathcal{K} = k) \approx \hat{y}_k = \frac{|\Omega_k|}{|\Omega|} \quad (11)$$

Also, we express the conditional entropy of the learned features as follows :

$$\begin{aligned}\mathcal{H}(\mathcal{F}|\mathcal{K}) &= \sum_k^K \mathbb{P}(\mathcal{K} = k) \mathcal{H}(\mathcal{F}|\mathcal{K} = k) \\ &\approx \frac{1}{|\Omega|} \sum_k^K |\Omega_k| \mathcal{H}(\mathcal{F}|\mathcal{K} = k)\end{aligned}\quad (12)$$

with each  $\mathcal{H}(\mathcal{F}|\mathcal{K} = k)$  given by :

$$\mathcal{H}(\mathcal{F}|\mathcal{K} = k) = - \int_{\mathbf{f}^\theta} \mathbb{P}(\mathbf{f}^\theta|\mathcal{K} = k) \log \mathbb{P}(\mathbf{f}^\theta|\mathcal{K} = k) d\mathbf{f}^\theta \quad (13)$$

Hereafter, for notation simplicity, we omit  $\mathcal{K}$  and use  $\mathcal{H}(\mathcal{F}|k)$  instead of  $\mathcal{H}(\mathcal{F}|\mathcal{K} = k)$ . Also, we use  $\mathbb{P}(\mathbf{f}^\theta|k)$  instead of  $\mathbb{P}(\mathbf{f}^\theta|\mathcal{K} = k)$ .

To estimate the conditional entropy in Eq. (13), let us refer to the following well known Monte-Carlo estimation [10,23] :

**Monte-Carlo estimation.** For any discrete set of points  $\mathbf{S} \subset \Omega$ , any function  $g$  and any feature embedding  $\mathbf{f}$ , we have :

$$\int_{\mathbf{f}} g(\mathbf{f}) \mathbb{P}(\mathbf{f}|\mathbf{S}) \approx \frac{1}{|\mathbf{S}|} \sum_{i \in \mathbf{S}} g(\mathbf{f}_i) \quad (14)$$

where  $\mathbf{f}_i$  denotes a feature vector at point  $i$ , and  $\mathbb{P}(\mathbf{f}|\mathbf{S})$  stands for the density of  $\{\mathbf{f}_i, i \in \mathbf{S}\}$ .

Therefore, applying Monte-Carlo to  $\mathcal{H}(\mathcal{F}|k)$  in Eq. (13), we can re-write Eq. (12) as follows :

$$\mathcal{H}(\mathcal{F}|\mathcal{K}) \approx - \frac{1}{|\Omega|} \sum_k^K \sum_{i \in \Omega_k} \log(\mathbb{P}(\mathbf{f}_i^\theta|k)) \quad (15)$$

Furthermore, using Bayes rule  $\mathbb{P}(\mathbf{f}_i^\theta|k) \propto \frac{p_{ik}}{\hat{p}_k}$ , in addition to the fact that  $\sum_{i \in \Omega_k} \log(\hat{p}_k) = |\Omega_k| \log(\hat{p}_k)$ , we obtain :

$$\begin{aligned}\mathcal{H}(\mathcal{F}|\mathcal{K}) &\approx - \frac{1}{|\Omega|} \sum_k^K \sum_{i \in \Omega_k} \log\left(\frac{p_{ik}}{\hat{p}_k}\right) \\ &= - \frac{1}{|\Omega|} \sum_k^K \sum_{i \in \Omega_k} \log(p_{ik}) + \frac{1}{|\Omega|} \sum_k^K \sum_{i \in \Omega_k} \log(\hat{p}_k) \\ &= \text{CE} + \frac{1}{|\Omega|} \sum_k^K |\Omega_k| \log(\hat{p}_k) \\ &= \text{CE} + \sum_k^K \hat{y}_k \log(\hat{p}_k)\end{aligned}\quad (16)$$

Finally, due to the definition of the label-marginal KL divergence, we have :

$$\mathcal{D}_{\text{KL}}(\mathbf{y}||\mathbf{p}) = \sum_{k=1}^K \hat{y}_k \log \left( \frac{\hat{y}_k}{\hat{p}_k} \right) \stackrel{\text{c}}{=} - \sum_k^K \hat{y}_k \log(\hat{p}_k) \quad (17)$$

This yields :

$$\text{CE} \stackrel{\text{c}}{=} \mathcal{H}(\mathcal{F}|\mathcal{K}) + \mathcal{D}_{\text{KL}}(\mathbf{y}||\mathbf{p}) \quad (18)$$

In summary, we give an information-theoretic prospective of CE. The entropy term can be considered as a ground-truth matching term, while the label-marginal KL term avoids trivial solutions and encourages the proportions of the predicted segmentation regions to match the ground-truth proportions.

## B The binary segmentation case

In the two-class (binary) segmentation case, Dice might be used for the foreground region only [19]. Similarly to the multi-class case discussed in the paper, a single Dice term also decomposes into a ground-truth matching term and label-marginal penalty, with the latter encouraging extremely imbalanced binary segmentations. For this specific case, the logarithmic Dice and CE could be written as summations over the foreground and background segmentation regions:

$$-\log(\text{Dice}_1) \stackrel{\text{c}}{=} \underbrace{-\log \left( \frac{1}{|\Omega_1|} \sum_{i \in \Omega_1} p_{i1} \right)}_{\text{Foreground matching: DF}_1} + \underbrace{\log \left( \sum_{i \in \Omega} p_{i1} + |\Omega_1| \right)}_{\text{Label-marginal bias: DB}_1} \quad (19)$$

$$\text{CE} = \underbrace{-\frac{1}{|\Omega_1|} \sum_{i \in \Omega_1} \log p_{i1}}_{\text{Foreground matching: CE}_1} - \underbrace{\frac{1}{|\Omega_2|} \sum_{i \in \Omega_2} \log(1 - p_{i1})}_{\text{Background matching: CE}_2} \quad (20)$$

In Eq. (19), the term  $\text{DB}_1$  can be expressed, up to an additive constant, as a function of the marginal probability of the foreground class ( $k = 1$ ) as follows:

$$\text{DB}_1 \stackrel{\text{c}}{=} \log(\hat{p}_1 + \hat{y}_1) \quad (21)$$

Clearly, the marginal probability  $\hat{p}_1$  measures the predicted proportion of pixels within the foreground region. This term reaches its minimum when the foreground region is empty ( $p_{i1} = 0 \forall i$ ). Therefore, since  $\log$  is monotonically increasing, minimizing term  $\text{DB}_1$  in Eq. (19) introduces a bias preferring small foreground structures. Note that this label-marginal term in the logarithmic Dice loss is important to avoid trivial solutions: when using the foreground-matching term alone, the model may assign all the pixels in the image to the foreground region.

The foreground-matching terms,  $CE_1$  and  $DF_1$ , are closely related, with the former being an upper bound on the latter, due to Jensen’s inequality:  $DF_1 \leq CE_1$ . Both foreground-matching terms are monotonically decreasing functions of each softmax and reach their global minimum when all the softmax predictions in the ground-truth foreground are equal to 1 (i.e., reach their target). Hence, the matching terms in Dice and CE can be viewed as two different penalty functions for imposing the same equality constraints,  $p_{i1} = 1, \forall i \in \Omega_1$ , thereby encouraging the predicted foreground to include the ground-truth foreground.

## C The temperature scaling

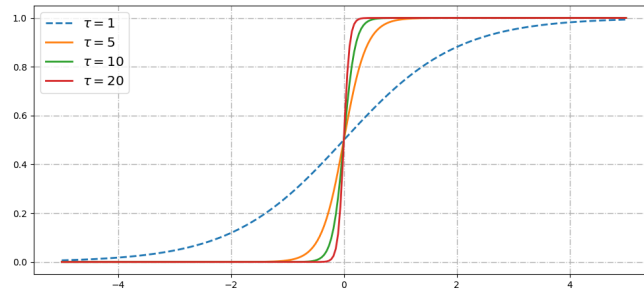


**Fig. 5. Comparison of soft-max functions with different temperature scaling parameter  $\tau$ .** It is shown that the confidence of the output increases with larger  $\tau$ . Best seen in color.

In our implementation, we employ a modified soft-max function with a temperature scaling parameter when computing the predicted region proportion  $\hat{p}_k$  (also referred to as the predicted label-marginal probability, as in Table 1 of the main text) :

$$s(\mathbf{z})_i = \frac{e^{\tau \cdot z_i}}{\sum_j^K e^{\tau \cdot z_j}} \quad (22)$$

where  $\mathbf{z} = (z_i)_{1 \leq i \leq K}$  is the input vector of the soft-max function, and  $\tau > 0$  acts as the temperature hyper-parameter. High values of  $\tau > 0$  yield high confidence of the soft-max prediction, as shown in Fig. 5: They push the soft-max vector towards the vertices of the simplex, with prediction values approaching either 0 or 1. As a result, this enables a better estimate of the actual region proportion (or relative size). Note, we set  $\tau$  to 10 throughout all our experiments.

## D Per-class results on Cityscapes test set

In Table 6, we report the detailed per-class results on the Cityscapes test set. The proposed methods outperform related losses on both network settings. In

**Table 6. Per-class Results on Cityscapes test set.** (Top: *Res50-FPN*, Bottom: *Res101-FPN*) The second row indicates the average region proportion (mRegProp) for each class. mIoU denotes the mean IoU score over all classes.

	road	swalk	build.	wall	fence	pole	tlight	sign	veg.	terrain	sky	person	rider	car	truck	bus	train	mbike	bike	mIoU
mRegProp (%)	32.6	5.4	20.2	0.6	0.8	1.1	0.2	0.5	14.1	1.0	3.6	1.1	0.1	6.2	0.2	0.2	0.2	0.1	0.4	
CE	97.5	79.3	90.3	45.0	<b>46.3</b>	53.5	61.6	67.3	<b>92.1</b>	70.1	93.5	78.4	53.3	<b>93.7</b>	41.4	48.8	38.2	55.2	67.1	67.0
Focal loss	<b>97.6</b>	79.1	89.8	41.3	43.6	49.9	57.7	63.8	91.7	68.4	94.1	75.7	47.3	93.0	37.8	44.9	35.6	50.5	63.8	64.5
1 – Dice	96.6	77.7	88.4	40.9	43.7	<b>55.5</b>	<b>68.5</b>	<b>71.2</b>	91.3	<b>70.9</b>	94.2	<b>80.4</b>	<b>57.6</b>	92.6	0.0	42.7	14.2	54.8	<b>69.6</b>	63.7
– log Dice	94.4	71.7	85.2	30.8	34.8	48.5	63.1	66.2	89.4	66.9	88.6	75.1	49.0	89.6	22.1	31.1	21.1	43.0	65.0	59.8
DiceCE	97.2	78.9	90.2	<b>45.5</b>	<b>46.4</b>	53.3	62.4	67.7	92.0	70.8	93.1	78.2	53.0	93.5	39.8	50.6	31.9	54.3	66.8	66.6
LogDiceCE	97.4	79.2	90.3	43.8	45.0	55.1	67.0	70.3	91.8	70.0	94.0	79.4	56.0	93.3	39.7	50.8	32.2	51.2	68.1	67.1
Ours ( $\mathcal{D}_{KL}$ )	<b>97.6</b>	<b>79.6</b>	<b>90.4</b>	45.2	45.0	53.1	61.3	66.9	92.0	70.5	94.1	78.5	54.7	93.6	<b>48.8</b>	<b>59.1</b>	45.8	<b>55.5</b>	67.0	<b>68.4</b>
Ours ( $\mathcal{L}_1$ )	<b>97.6</b>	79.4	<b>90.4</b>	44.1	45.8	53.7	61.3	67.2	<b>92.1</b>	70.2	<b>94.3</b>	78.8	54.4	<b>93.7</b>	47.8	58.4	<b>46.8</b>	55.4	67.3	<b>68.4</b>
CE	97.8	81.3	90.9	45.6	50.2	55.7	64.2	67.1	92.3	70.9	94.6	79.7	57.6	94.2	51.7	58.0	43.5	58.1	68.5	69.6
Focal loss	97.9	81.3	90.6	46.4	46.9	52.4	59.9	65.7	91.9	69.4	94.4	77.3	53.0	93.6	42.7	48.7	35.9	54.5	66.5	66.8
1 – Dice	96.9	79.0	88.2	0.0	48.0	56.7	<b>69.6</b>	<b>72.2</b>	91.3	<b>71.3</b>	94.1	<b>81.3</b>	<b>62.9</b>	92.5	26.5	0.0	27.8	0.0	<b>70.7</b>	59.4
– log Dice	95.8	73.5	86.5	33.0	37.1	50.2	63.5	66.6	89.7	67.6	92.0	77.1	52.2	90.8	32.0	37.5	26.5	50.4	67.9	62.6
DiceCE	97.9	81.9	91.1	45.4	48.1	<b>57.8</b>	69.1	72.1	91.3	71.2	<b>94.8</b>	80.1	61.6	93.0	44.7	55.8	38.8	58.0	70.9	69.7
LogDiceCE	97.7	80.0	90.5	43.8	48.5	55.8	68.1	70.9	91.7	70.5	94.2	80.6	61.4	93.7	46.9	57.6	40.6	<b>59.2</b>	70.4	69.6
Ours ( $\mathcal{D}_{KL}$ )	97.9	81.4	91.2	<b>48.7</b>	49.7	55.5	63.7	68.6	<b>92.4</b>	70.6	94.6	79.9	57.1	<b>94.3</b>	<b>54.5</b>	<b>61.1</b>	43.5	58.3	68.4	<b>70.1</b>
Ours ( $\mathcal{L}_1$ )	<b>98.0</b>	<b>81.9</b>	<b>91.2</b>	<b>48.7</b>	<b>50.3</b>	55.7	63.8	68.3	92.3	70.7	94.5	79.8	57.5	94.2	52.9	60.3	<b>44.0</b>	<b>59.2</b>	68.7	<b>70.1</b>

term of mIoU, we achieve 68.4% and 70.1% on Res50-FPN and Res101-FPN, respectively. Compared to the baseline CE, our method yields improvement for most of the minority classes, like fence, train and motorbike, while it shows better adaptability for diverse classes than the Dice loss.